Sintering and carbidization under simulated high conversion on a cobalt-based Fischer-Tropsch catalyst; manganese oxide as a structural promotor

van Koppen, Luke M.; Iulian Dugulan, A.; Hensen, Emiel J.M.; Bezemer, G. Leendert

DOI
10.1016/j.jcat.2022.06.020

Publication date
2022

Document Version
Final published version

Published in
Journal of Catalysis

Journal of Catalysis 413 (2022) 106–118

Contents lists available at ScienceDirect

Journal of Catalysis

journal homepage: www.elsevier.com/locate/jcat

Sintering and carbidization under simulated high conversion on a cobalt-based Fischer-Tropsch catalyst; manganese oxide as a structural promotor

Luke M. van Koppen [a,b], A. Iulian Dugulan [b], G. Leendert Bezemer [c], Emiel J.M. Hensen [b,*]

[a] Laboratory of Inorganic Materials and Catalysis, Department of Chemical Engineering and Chemistry, Eindhoven University of Technology, Het Kranenveld 14, 5600 MB Eindhoven, the Netherlands

[b] Laboratory of Fundamentals Aspects of Materials and Energy, Department of Radiation Science & Technology, Technical University of Delft, Mekelweg 15, 2628 CD Delft, the Netherlands

[c] Energy Transition Campus Amsterdam, Shell Global Solutions International B.V., Grasweg 31, 1031 HW Amsterdam, the Netherlands

ARTICLE INFO

Article history:
Received 18 March 2022
Revised 8 June 2022
Accepted 10 June 2022
Available online 14 June 2022

Keywords:
Fischer-Tropsch synthesis
Cobalt
Deactivation
Manganese oxide
Mössbauer spectroscopy

ABSTRACT

The commercial application of cobalt-based Fischer-Tropsch synthesis (FTS) suffers from catalyst deactivation. One of the main deactivation mechanisms under industrial conditions is sintering. In this work, we explored the role of manganese oxide as a structural promoter against sintering in a carbon nanofiber supported cobalt model catalyst. We employed *in situ* Mössbauer emission spectroscopy to study cobalt sintering in synthesis gas as a function of the steam partial pressure, which mimics high CO conversion during FTS. Steam accelerates the sintering of non-promoted metallic cobalt particles. Model experiments point to a synergistic effect between carbon monoxide and steam on cobalt sintering. In the mangense-promoted case, sintering is significantly reduced, indicative of the structural stabilization of small cobalt particles by manganese oxide. Nevertheless, a fraction of cobalt particles in close interaction with manganese oxide carburized under these conditions, resulting in a lower catalytic activity.

1. Introduction

Fischer-Tropsch synthesis, which refers to the conversion of synthesis gas to fuels and chemicals, is of growing importance for the valorization of diverse feedstocks. At the molecular level, Fischer-Tropsch synthesis (FTS) entails surface-catalyzed polymerization of *in situ* produced CH_x monomers formed by dissociation of adsorbed CO and subsequent hydrogenation of adsorbed carbon species [1]. There are currently two kinds of commercially viable low temperature FT catalysts based on either cobalt or iron. Cobalt catalysts are characterized by higher activity, higher chain-growth probability, and lower byproduct formation in comparison to iron catalysts. Moreover, different from iron, cobalt shows only very low activity in the water–gas shift reaction [2]. Therefore, cobalt catalysts are preferred when the synthesis gas is derived from natural gas and longer chain paraffins, and olefins are targeted. Whilst cobalt-based Fischer-Tropsch has many advantages, it also suffers from a strong particle size effect, requiring catalysts with a relatively high dispersion with an optimum around 6–8 nm [3] and good stability for successful exploitation [4].

Catalyst deactivation in cobalt-based Fischer-Tropsch synthesis is a major challenge, as catalyst replacement in the commonly deployed fixed-bed reactors can result in several weeks of interrupted production combined with the relatively high cost of cobalt. Therefore, improving the stability of cobalt-based FTS catalysts would be a substantial benefit in the commercial operation of the Fischer-Tropsch process [4]. Catalyst deactivation in cobalt-based Fischer-Tropsch is a complex process, which according to the state of the art can be categorized in long- and short-term deactivation profiles [5]. Deactivation after the start-up of the reaction has been studied extensively with every resurgence of Fischer-Tropsch research [4,6,7]. The short-term deactivation is often found to be reversible under mild hydrogen treatments [8]. In contrast, the long-term deactivation cannot be reversed, making it of operational significance. The complexity lies in the underlying causes of deactivation, which are many and range from poisoning to strong metal support interaction (SMSI) [4]. Poisoning is avoided industrially by extensive scrubbing of the feed and the use of proper guarding technology and can therefore usually be excluded as a reason for deactivation under realistic conditions. This leaves

* Corresponding author.
E-mail address: e.j.m.hensen@tue.nl (E.J.M. Hensen).

https://doi.org/10.1016/j.jcat.2022.06.020
0021-9517/

oxidation, SMSI, carbon deposits and sintering as mechanisms for long-term catalyst deactivation.

Sintering of the active metallic cobalt phase is typically found to be one of the main reasons for deactivation under FTS conditions [9–11]. Carbon nanofibers (CNF) as a support have an advantage in studying the sintering mechanism. As a result of the weak interaction between the support and the metallic cobalt phase, sintering occurs on a much shorter timescale [12–15]. Carbon nanofiber catalysts have previously been used as model systems in order to understand the effect of cobalt particle size, and catalyst deactivation in Fischer-Tropsch synthesis [3,8,16–18]. The role of water, a main product in FTS, on deactivation has been under earlier investigation and studies have shown the potential impact on oxidation as well as sintering. Thermodynamic calculations have shown that spherical cobalt nanoparticles smaller than 4.4 nm are likely to be oxidised at the prevailing H_2O/H_2 ratio at FTS conditions [19]. Experimental investigations, however, not always detect bulk oxidation of cobalt under these (simulated) industrial FTS conditions which can be related to e.g. usage of larger cobalt particles, which are more resistant to oxidation, or the kinetic hindrance of water splitting [4,16,20–22]. The role of water on sintering has been established more convincingly. For instance, Kliewer et al. proposed that partial oxidation of cobalt by water led to oxide/hydroxide species prone to coalescence on a wetted support [12]. The group of Khodakov suggested a similar mechanism for the faster sintering of cobalt observed in the presence of water [23], whereas Ostwald ripening by sub-carbonyl species in the presence water has been hypothesized by Moodley et al. [6]. Additionally, recent *in situ* studies have shown that the formation of bulk cobalt carbides is possible under realistic Fischer-Tropsch conditions [24–26], although the process seems strongly kinetically inhibited. The formation of these cobalt carbides was reported to lead to a decrease in activity and an increase in methane selectivity [24].

Herein, we investigate the role of water on the deactivation of CNF-supported cobalt and manganese oxide-promoted cobalt catalysts. Manganese oxide has been investigated as a constituent of cobalt-based FTS catalysts already in the first half of the 20th century [27]. These early results showed the potential of manganese to reduce methane selectivity. Later pioneering studies using catalysts prepared by co-precipitation of cobalt and manganese improved our understanding of the role of manganese oxide as a support and selectivity promoter [28–31]. More recent work focused on manganese oxide as a promoter for supported cobalt FTS catalysts [32–35], in which a positive impact on the chain-growth probability was observed. In the present work, we address the role of manganese oxide as a structural promoter to reduce cobalt sintering. Sintering of cobalt is investigated under actual reaction conditions at elevated pressure by *in situ* Mössbauer emission spectroscopy (MES) [36]. A previous ^{57}Co MES study showed that water increases cobalt sintering [16]. The MES measurements are supplemented by XPS, TEM and STEM-EDX characterization, while the catalytic performance is measured in a microflow reactor.

2. Experimental section

2.1. Catalyst preparation

Carbon nanofibers (CNF) (surface area 200 m^2g^{-1}, total pore volume of 0.46 mL g^{-1}) were synthesized according to literature [37]. All the supported catalysts were prepared by incipient wetness impregnation preparation followed by drying in air at 120 °C for 6 h. The impregnation solutions were obtained by dissolving the appropriate amount of $Co(NO_3)_2{\cdot}6H_2O$ (≥98.0%, Sigma Aldrich) and $Mn(NO_3)_2{\cdot}3H_2O$ (≥97.0%, Sigma Aldrich) in dehydrated ethanol. Two catalysts were prepared with a cobalt loading of 4 wt%, one unpromoted and the other promoted by manganese oxide in a Co/Mn atomic ratio of 5. These samples are denoted by Co(4)/CNF and Co(4)Mn/CNF, respectively. Another Co-Mn catalyst with a cobalt loading of 10 wt% Co and the same Co/Mn ratio of 5 is denoted by Co(10)Mn/CNF. A part of the impregnation solutions was spiked with radioactive ^{57}Co by adding an appropriate amount of a solution containing 90 MBq ^{57}Co in 0.1 M HNO_3, while the other part was spiked with the same amount of a 0.1 M HNO_3 solution without radioactive cobalt. In this way, two comparable samples were obtained with nearly identical cobalt loading, one being doped with approximately 0.3 μg of ^{57}Co for the Mössbauer measurements. The radioactive samples were used for Mössbauer spectroscopy.

2.2. Characterization

2.2.1. Electron microscopy

The surface average particle size and particle size distribution were determined with transmission electron microscopy (TEM). TEM measurements were performed on a FEI Tecnai 20 electron microscope operated at an electron acceleration voltage of 200 kV with a LaB_6 filament. Typically, a small amount of the sample was ground and suspended in pure ethanol, sonicated, and dispersed over a Cu grid with a holey carbon film.

The nanoscale distribution of elements in the samples was studied using scanning transmission electron microscopy – energy-dispersive X-ray spectroscopy (STEM-EDX). Measurements were carried out on a FEI cubed Cs-corrected Titan operating at 300 kV. Samples were crushed, sonicated in ethanol, and dispersed on a holey Cu support grid. Elemental analysis was done with an Oxford Instruments EDX detector X-MaxN 100TLE.

2.2.2. In situ Mössbauer emission spectroscopy

Mössbauer emission spectroscopy (MES) was carried out at different temperatures using a constant acceleration spectrometer set up in a triangular mode with a moving single-line $K_4Fe(CN)_6{\cdot}3H_2O$ absorber enriched in ^{57}Fe. The velocity scale was calibrated with a ^{57}Co:Rh source and a sodium nitroprusside absorber. Zero velocity corresponds to the peak position of the $K_4Fe(CN)_6{\cdot}3H_2O$ absorber measured with the ^{57}Co:Rh source, positive velocities corresponding to the absorber moving towards the source.

To be able to measure under *in situ* Fischer-Tropsch conditions, an earlier described high pressure MES cell is used [36]. The cell is equipped with a beryllium window above the sample cup which ensures a leak tight system whilst still allowing the gamma rays to pass through. Additionally, the use of water cooling as well as various O-rings allow this cell to pass all safety requirements of working with radiation and high pressures of dangerous gasses. Furthermore, the use of a metal mesh in the sample cup means both the radioactive probed catalyst as well as a non-radioactive counterpart can be loaded simultaneously without mixing. In this way the non-radioactive counterpart will experience the exact same conditions and make it possible to perform *ex situ* characterization on a used catalyst sample.

The Mössbauer spectra were fitted using the MossWinn 4.0 program [38]. The spectra of very small superparamagnetic species were fitted using the two-state magnetic relaxation model of Blume and Tjon, which assumes the presence of a fluctuating magnetic field that jumps between the values of + H and -H along the z-axis with an average frequency τ [39]. Here H typically equals 500 kOe and τ can vary between 1.10^{-9} and 1.10^{-12} s^{-1}. The Mössbauer spectra of larger particles were fitted using a hyperfine sextuplet, resulting from the local magnetic field experienced by bulk metallic particles. The experimental uncertainties in the calculated

Mössbauer parameters, estimated using Monte Carlo iterations by the MossWinn 4.0 program, were as follows: IS and QS ± 0.01 m m s^{-1} for the isomer shift and quadrupole splitting, respectively; ± 3% for the spectral contribution; ± 3 kOe for the hyperfine field.

Typically, 500 mg of radioactively probed and 100 mg of non-radioactive catalyst (sieve fraction 250–500 μm) was loaded into the reactor cell. Fischer-Tropsch experiments were performed *in situ* following reduction at 350 °C for 2 h in 100 mL/min flow of pure H_2. Reactions were done at 200 °C and 20 bars of pressure, the CO/H_2 was kept at 4 throughout, and steam was fed to achieve different relative humidities. Experiments were typically performed for 2 days; however, to achieve a significant degree of oxidation at industrially relevant conditions this length was increased to 5 and 11 days for the treatments with a relative humidity of 25 and 57% respectively. The water was evaporated and mixed with the incoming feed gas using a Bronkhorst CEM W-102A-222 K. Wax products were collected in a downstream hot catch pot, and water was retrieved in a subsequent cold catch pot. An online Trace GC Ultra from ThermoFischer equipped with a RT-Silica bond column and a flame ionization detector and a Stabilwax column and a thermal conductivity detector was used to analyse the gaseous Fischer-Tropsch products.

2.2.3. Quasi in situ X-ray photoelectron spectroscopy (XPS)

The oxidation state of cobalt and manganese was studied by *quasi in situ* XPS using a Kratos AXIS Ultra 600 spectrometer equipped with a monochromatic Al Kα X-ray source (Al Kα 1486.6 eV). Survey scans were recorded at a pass energy of 160 eV, detailed region scans at 40 eV. The step size was 0.1 eV and the background pressure during the measurements was kept below 10^{-9} mbar.

A high-temperature reaction cell (Kratos, WX-530) was used to pre-treat the sample supported on an alumina stub, allowing *in vacuo* sample transfer into the analysis chamber. Reduction was performed in a pure H_2 flow at atmospheric pressure and 350 °C for 2 h. After reduction, the reaction cell was evacuated to a pressure below 10^{-9} mbar. Then, the sample was cooled to 150 °C and transferred to the analysis chamber. Data analysis was done with the CasaXPS software (version 2.3.22PR1.0). The binding energy scale was corrected for surface charging by taking the C 1 s peak of adventitious carbon as a reference at 284.8 eV.

2.3. Catalytic activity measurements

The catalytic performance was determined in a single-pass flow reactor system (Microactivity Reference unit, PID Eng&Tech) operated at a temperature of 220 °C or 240 °C, a total pressure of 20 bar and a H_2/CO ratio of 4. In a typical experiment, 50 mg of catalyst (sieve fraction 125–250 μm) mixed with SiC particles of the same sieve fraction was placed in a tubular reactor with an internal diameter of 9 mm. The temperature was controlled via a thermocouple, located in the centre of the catalytic bed. The reactor was first heated in a flow of H_2 to 350 °C at a rate of 5 °C/min. After a dwell time of 2 h, the reactor was cooled to 220 °C and the gas feed composition was changed to reaction conditions. A gas-hourly space velocity (GHSV) of 1000 h^{-1} was applied which resulted in a CO conversion of about 10 ± 5%. A TRACE1300 GC from Scientific instrument equipped with a RT-Silica bond column and a flame ionization detector, and a Porabond-Q column and a thermal conductivity detector was used to measure the products in the reactor effluent. The Weisz – Prater criterion was calculated to confirm operations did not run under internal mass transfer limitations. Under the applied reaction conditions, the production of CO_2 was not detected and the selectivity toward oxygenates on a molar carbon basis was less than 1%. Liquid products and waxes were collected in a downstream cold trap. To calculate the CO conversion independent of volume changes, the feed contained a known amount of Ar (i.e., 9 vol% Ar in CO was used). The CO (X_{CO}) conversion was determined in the following manner:

$$X_{CO} = 1 - \frac{F_{Ar,in}F_{CO,out}}{F_{CO,in}F_{Ar,out}}$$

where $F_{Ar,in}$ is the volumetric Ar flow in the reactor feed, $F_{CO,in}$ is the volumetric CO flow in the reactor feed, $F_{Ar,out}$ and $F_{CO,out}$ are the respective volumetric flows of Ar and CO out of the reactor system.

The carbon-based selectivity of hydrocarbon compound C_i (S_{Ci}) was calculated using:

$$S_{Ci} = \frac{F_{Ar,in}F_{Ci}v_i}{F_{Ar,out}F_{CO,in}X_{CO}}$$

where F_{Ci} is the volumetric flow of hydrocarbon compound C_i out of the reactor, and v_i is the stochiometric factor of the hydrocarbon compound.

The cobalt time-yield (CTY) was determined using the following equation:

$$CTY = \frac{F_{CO,in}X_{CO}}{m_{Co}}$$

where m_{Co} is the weight of cobalt used in the catalytic reaction. These equations were also used to analyse the activity measured during *in situ* Mössbauer experiments.

3. Results and discussion

3.1. Fresh catalyst characterization

Fig. 1 shows representative TEM images of the as-prepared Co(4)/CNF, Co(4)Mn/CNF and Co(10)Mn/CNF catalysts. The images clearly show small cobalt oxide nanoparticles dispersed on the fibrous carbon strands of the support. The average size and size distribution of the cobalt phase were determined by measuring the size of about 150 particles in ca. 8 TEM images per sample. The average particle sizes of the Co(4)/CNF and Co(4)Mn/CNF samples were 4.0 ± 2.7 nm and 5.6 ± 3.3 nm, respectively. Thus, the presence of manganese oxide did not substantially affect the particle size of the cobalt phase in the catalyst precursor. The particles in the Co(10)Mn/CNF sample with a higher cobalt loading were larger with an average size of 11.8 ± 5.4 nm.

Mössbauer spectra measured for the fresh catalysts are shown in Fig. 2a. All spectra contain a doublet corresponding to oxidic cobalt. This feature has an isomer shift (IS) of 0.2 mm s^{-1} and a quadrupole splitting (QS) of 0.7 mm s^{-1}, which can be assigned to Co^{3+}. The spectrum of the non-promoted Co(4)/CNF catalyst shows a secondary doublet with a spectral contribution of approximately 17%, an IS of 1.0 mm s^{-1} and a QS of 2.2 mm s^{-1}. These Mössbauer parameters are due to Co^{2+}. The observation of two different electronic states of cobalt in the fresh catalysts comes from the Auger cascade that follows the decay of the ^{57}Co probe [40–43]. It is important to note that both Co^{3+} and Co^{2+} contributions have been observed by MES in ^{57}Co-doped CoO, a compound in which all cobalt, before nuclear decay, is divalent [40]. This happens because the neighbouring Co^{2+} atoms can stabilize Co^{3+} formed during the Auger cascade of ^{57}Co long enough to be measured. As ^{57}Co probe atoms with more neighbouring Co^{2+} atoms are more likely to stabilize Co^{3+}, this contribution can provide qualitative information about the dispersion of oxidic cobalt [44–46]. For instance, the increasing contribution of the Co^{3+} doublet with increasing cobalt loading on an alumina support could be attributed to a lower dispersion of cobalt oxide [47]. In the spectra of the fresh catalysts, we find the highest contribution of Co^{2+} for the non-promoted Co(4)/CNF sample. This suggests that this catalyst has the highest

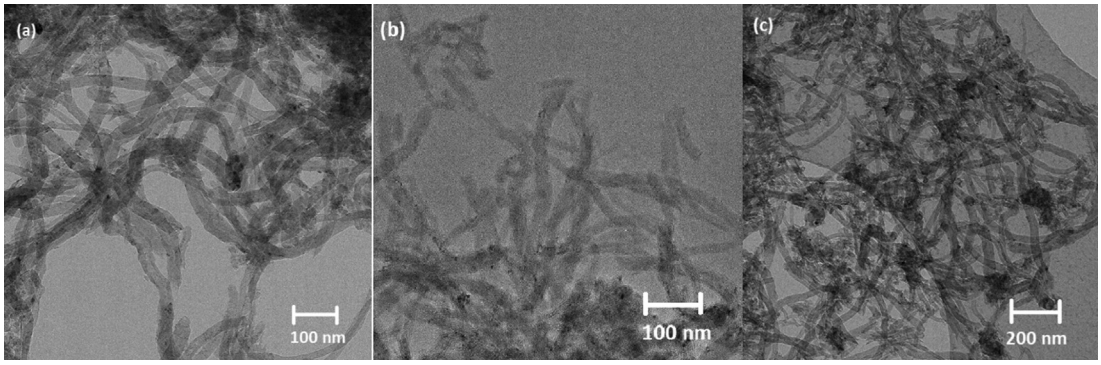

Fig. 1. Representative TEM images of from left to right the as prepared (a) Co(4)/CNF, (b) Co(4)Mn/CNF, and (c) Co(10)Mn/CNF.

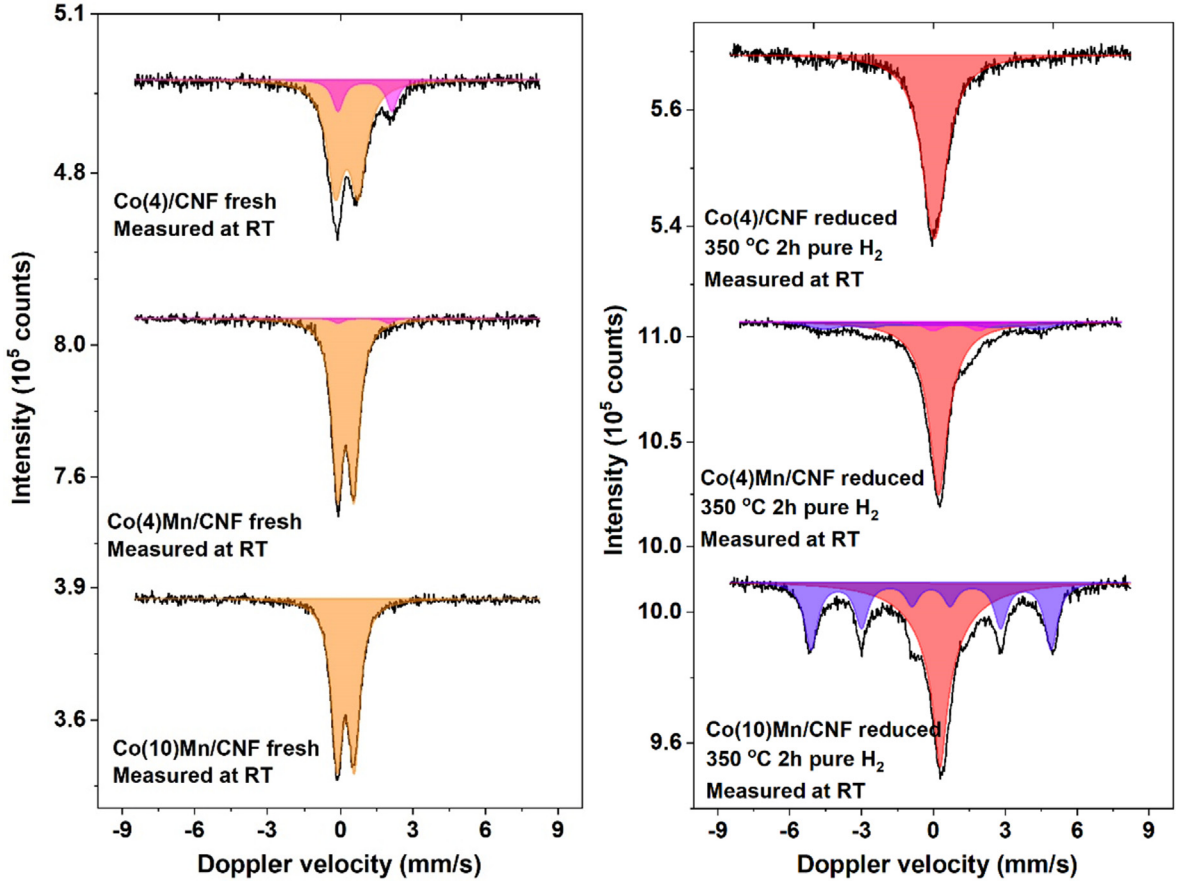

Fig. 2. (a) Mössbauer spectra of fresh Co(4)/CNF, Co(4)Mn/CNF, and Co(10)Mn/CNF catalysts: black lines represent the experimental spectra, orange and magenta the fitted cobalt oxide doublets. (b) Mössbauer spectra of reduced Co(4)/CNF, Co(4)Mn/CNF, and Co(10)Mn/CNF catalysts at 350 °C, for 2 h under pure hydrogen: black lines represent the experimental spectra, red the fitted metallic cobalt SPM singlet, blue the fitted bulk metallic cobalt sextuplet, and magenta the fitted cobalt oxide doublet. (For interpretation of the references to colour in this figure legend, the reader is referred to the web version of this article.)

dispersion of oxidic cobalt. The high Co loading catalyst shows no contribution of Co^{2+} due to the lower dispersion of cobalt oxide.

3.1.1. In situ Mössbauer spectroscopy of reduced catalysts

Mössbauer spectra of the catalysts after reduction at 350 °C are given in Fig. 2b. The singlet observed for the reduced Co(4)/CNF sample with an IS of 0.0 mm s^{-1} is due to metallic cobalt. The presence of such a singlet instead of a sextuplet demonstrates that cobalt is present as small cobalt metal particles without magnetic ordering (i.e., <6 nm) [16]. We will refer to this superparamagnetic (SPM) contribution as small metallic cobalt particles. The spectrum of the Co(4)Mn/CNF sample is different. It contains both singlet (ca. 76%) and sextuplet (ca. 17%) contributions of metallic cobalt. The sextuplet points to the presence of magnetically ordered cobalt metal particles, which is common for particles larger than 6 nm. The finding that this sample contains larger particles is in line with the TEM analysis (Fig. 1). The particles represented by this sextuplet will be referred to as large metallic cobalt particles. Furthermore, the spectrum contains a small contribution (7%) of cobalt oxide. The related doublet has an IS of 1.0 mm s^{-1} and a QS of 2.0 mm s^{-1}, which is indicative of small dispersed Co^{2+}-oxide particles that might be stabilized by their strong interaction with

manganese oxide, which does not reduce under our applied conditions [48]. The Mössbauer spectrum of the promoted sample with a higher cobalt loading, Co(10)Mn/CNF, contains the signatures of small and large cobalt particles. Compared to Co(4)Mn/CNF, the sextuplet contribution of large metallic cobalt particles is larger (ca. 44%), which is in line with the presence of larger particles as determined by TEM.

3.2. In situ Fischer-Tropsch Mössbauer emission spectroscopy

In situ Mössbauer spectra were recorded for the three catalysts as a function of the steam partial pressure at a temperature of 200 °C, a total pressure of 20 bar and a H_2/CO ratio of 4. The steam partial pressure will be expressed as the relative humidity at the applied conditions. In Table S1 the reactant flows at the different experimental conditions are provided. Spectra were recorded for at least 48 h at each humidity step except for the relative humidity of 25% and 57% where the durations were prolonged to 5 and 11 days, respectively. These two treatments were longer, these conditions are most industrially relevant for commercial fixed-bed FTS operation. Moreover, in performing these long-term humidity tests, we aimed to achieve a high degree of deactivation to better understand the underlying deactivation mechanisms. The reported values of the Mössbauer parameters for these prolonged treatments are obtained from the last two days at these conditions, to accurately report the state of the catalysts at the end of the test.

The spectra for the Co(4)/CNF sample exposed to these treatments contain two contributions of metallic cobalt (Fig. 3). The singlet has an IS of −0.2 mm s^{-1} (recorded at 200 °C), which corresponds to small metallic cobalt particles. The sextuplet representing large metallic cobalt particles has the same IS. The changes in the spectral contribution and hyperfine field (HF) of the sextuplet with increasing steam pressure provide qualitative information on the sintering behavior of the metallic cobalt phase. These and other Mössbauer parameters are given in Table S2. The increasing contribution of the sextuplet and concomitant decreasing contribution of the SPM phase clearly show that, with increasing relative humidity, small metallic cobalt particles sinter into larger ones. The increasing HF of the large metallic cobalt sextuplet underpins that the metallic cobalt particles grow when the humidity is increased. It is important to note that the extent of sintering was found to still be increasing during the last days on stream and would have further increased upon longer exposure time. As such the reported values do not reflect a fully deactivated catalyst. The tendency of cobalt sintering under humid FTS conditions is stronger than observed under non-reactive conditions in previous Mössbauer measurements performed on similar Co/CNF catalysts [16]. Previous studies suggest that the sintering of cobalt during FTS on graphite occurs exclusively through partially oxidized cobalt [49,50]. In our experiments we were unable to see any contributions of oxidic cobalt. However, the previously mentioned studies and the work of Moodley et al. [6] strongly suggests that this sintering occurs through an Ostwald ripening mechanism, which could explain why we are unable to see these short lived oxidic cobalt species as they migrate over the surface before re-reducing.

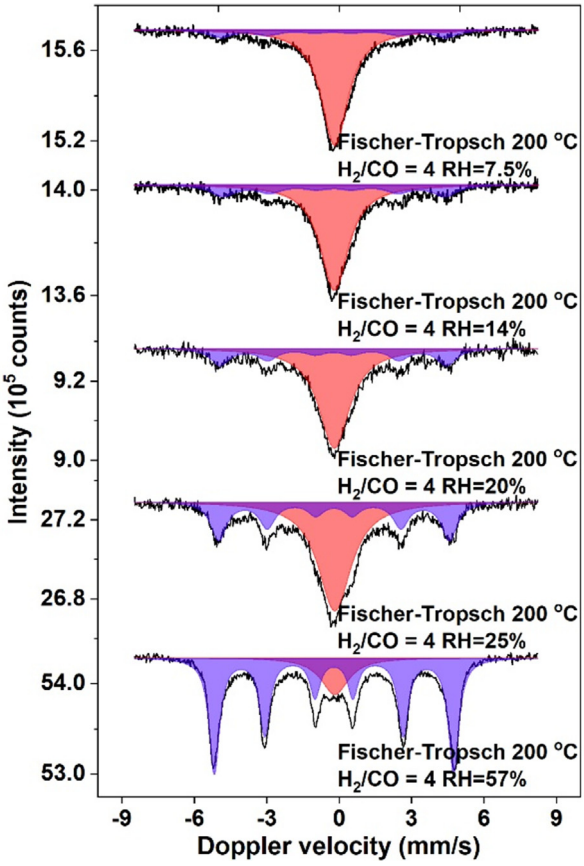

Fig. 3. *In situ* Mössbauer spectra measured of the Co(4)/CNF catalyst during FTS conditions under increasing humidity: black lines represent the experimental spectra, red the fitted metallic cobalt SPM singlet, and blue the fitted bulk metallic cobalt sextuplet. (For interpretation of the references to colour in this figure legend, the reader is referred to the web version of this article.)

Additional measurements were performed without CO in the feed to study the effect of exposure to a H_2O/H_2 mixture on the sintering of Co(4)/CNF. To this end, a freshly reduced Co(4)/CNF catalyst was exposed at 200 °C to a mixture of steam and hydrogen (molar ratio H_2O/H_2 = 1) diluted in two different flows of inert to achieve relative humidity of 25% and 57% respectively (Table S3). The spectra corresponding to these steam treatment conditions are given in Fig. 4. The SPM contributions in the freshly reduced catalysts differ slightly. Following an 11-day treatment at a relative humidity of 25%, the bulk cobalt contribution changed from 5% to 19% as measured at room temperature. At a higher relative humidity of 57%, the sextuplet contribution measured at room temperature increased from 12% after reduction to 41% after 11 days steam treatment. In Fig. 5, the impact of process conditions on the fraction of sintered cobalt is plotted as a function of the relative humidity. A clear trend is seen that exposure to more humid conditions results in an increased amount of sintered cobalt particles, which points to the detrimental effect of H_2O. A much more severe sintering is seen for the experiment where both CO and H_2O were present, which points to a synergy between steam and CO on cobalt sintering under FTS conditions. In the cobalt-catalyzed FT reaction, the simultaneous presence of both CO and water cannot be prevented, although the reaction conditions can be moderated to reduce the relative humidity and hence suppress the sintering rate. This is in agreement with previous results found by Claeys et al. [9], who reported enhanced sintering in the presence of both CO and steam for cobalt on an alumina support.

Spectra measured for the promoted Co(4)Mn/CNF catalyst are given in Fig. 6 and the corresponding Mössbauer fit parameters are listed in Table 1. Similar to the non-promoted Co(4)/CNF catalyst, these spectra show a singlet due to small metallic cobalt particles. The Co^{2+} contribution (7%) remaining after reduction indicates that reduction in the presence of manganese oxide is more difficult. This is in line with literature [32,51]. Complete reduction of the cobalt phase was obtained after the first FTS conditions without steam, although during this and subsequent humid treatments no reduction of the manganese oxide promotor is expected [48]. During the experiment and different from Co(4)/CNF without manganese oxide, this sample does not undergo

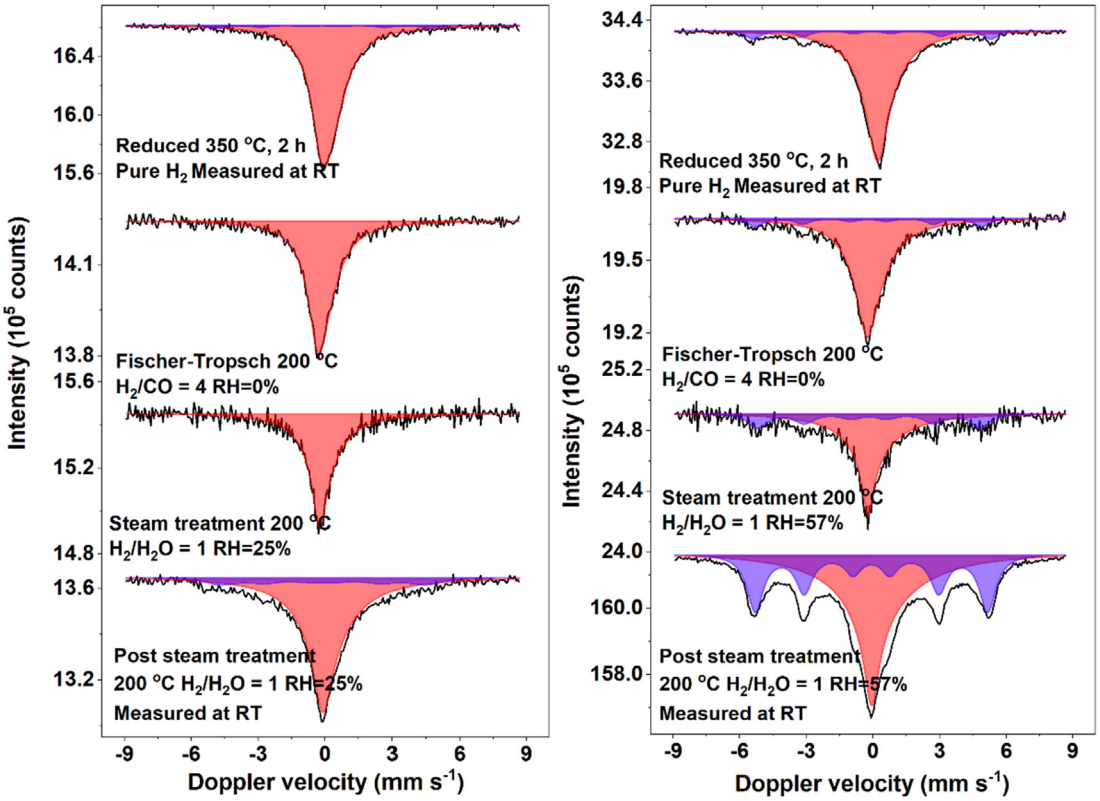

Fig. 4. (a) *In situ* Mössbauer spectra measured of the Co(4)/CNF catalyst before, during and after steam treatment with a relative humidity of 25%: black lines represent the experimental spectra, red the fitted metallic cobalt SPM singlet, and blue the fitted bulk metallic cobalt sextuplet. (b) *In situ* Mössbauer spectra measured of the Co(4)/CNF catalyst before, during and after steam treatment with a relative humidity of 57%: black lines represent the experimental spectra, red the fitted metallic cobalt SPM singlet, and blue the fitted bulk metallic cobalt sextuplet. (For interpretation of the references to colour in this figure legend, the reader is referred to the web version of this article.)

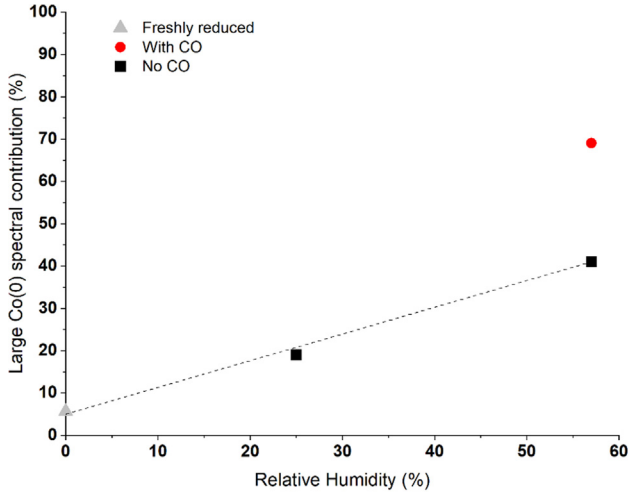

Fig. 5. The contribution of relatively large metallic cobalt particles determined by Mössbauer spectroscopy at room temperature of a freshly reduced catalyst (grey) and after treatment under humid conditions without CO (black) and with CO (red). (For interpretation of the references to colour in this figure legend, the reader is referred to the web version of this article.)

extensive sintering of small metallic cobalt particles into larger ones upon humid FTS treatments. Only after 11 days at the highest relative humidity of 57%, a contribution of larger cobalt particles is apparent from the observation of a sextuplet. Another difference with the manganese oxide-free sample is the appearance of a doublet with an IS of 0.0 mm s^{-1} and a QS of 0.8 mm s^{-1} (recorded at 200 °C) at a relative humidity of 14%. This doublet can be attributed to cobalt carbide species, analogous to the Fe_xC phase found in previous Mössbauer results [52]. This assignment was further confirmed by carbidizing a cobalt catalyst under pure CO, which resulted in a dominant carbide phase (60%) with the same Mössbauer parameters as shown in Figure S4 (IS = 0.1 mm s^{-1}, QS = 0.8 mm s^{-1}). Thus, the manganese oxide-promoted catalyst was partially carbidized under the given experimental conditions.

Table 1 shows how the spectral contribution of this cobalt carbide phase evolved with increasing relative humidity. While initially an increasing steam partial pressure resulted in more extensive carbidization, the contribution of carbidized species did not further increase when the relative humidity was raised above 25%. The contribution of the cobalt carbide phase was about 20%. Contrary to previously observed cobalt metal sintering, the spectral contribution of carbide did not further increase when the treatment was prolonged to 11 days. The contribution measured during the first two days (19%) was equal to the one found during the final two days of treatment. This shows that the carbide phase is formed relatively fast upon application of the humid FTS conditions. At the end of these measurements, the carbidized sample was reduced in pure H_2 at 350 °C for 2 h. The spectrum in Fig. 7 shows that the Co_2C phase was converted to large metallic cobalt particles as evident from growth of the sextuplet which is indicative of large cobalt nanoparticles. Comparing the spectra of the re-reduced Co(4)Mn/CNF sample with the non-promoted Co(4)/CNF sample subjected to the same humidity treatments shows that, after the same treatment, the promoted catalyst contains 60% small metallic cobalt nanoparticles, while this amounts to 31% for the unpromoted catalyst. This difference indicates that the cobalt particles in the unpromoted Co(4)/CNF catalyst have grown more than those in the promoted Co(4)Mn/CNF catalyst. These observations high-

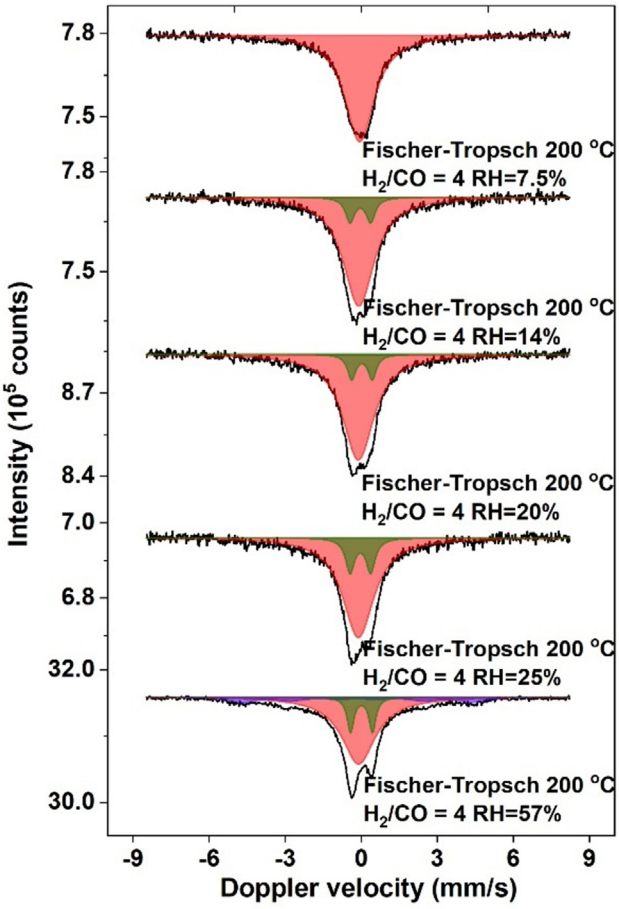

Fig. 6. *In situ* Mössbauer spectra measured of the Co(4)Mn/CNF catalyst during FTS conditions under increasing humidity: black lines represent the experimental spectra, red the fitted metallic cobalt SPM singlet, blue the fitted bulk metallic cobalt. (For interpretation of the references to colour in this figure legend, the reader is referred to the web version of this article.)

light that manganese oxide decreases sintering during humid FTS operation, although a small part of the metallic cobalt phase is carbidized.

Previous studies on carbon-supported cobalt catalysts have shown that direct oxidation by water of the metallic cobalt particles is kinetically hindered in the absence of CO [22]. However, when CO was introduced, rapid oxidation to cobalt oxide occurred. The authors proposed a mechanism in which removal of adsorbed oxygen due to CO dissociation is hindered by water. Whilst no oxidic cobalt is observed in our spectra, we find that part of cobalt carbidizes when both CO and steam are present. This carbidization might follow a similar mechanism as that postulated for oxidation, where carbon accumulates on the surface due to fast CO dissociation in the presence of the manganese oxide promoter and removal being hindered by water. The accumulation of carbon species on the surface would facilitate the formation of cobalt carbide. In a different study [24], it was shown that the formation of cobalt carbide can also occur under industrial FTS conditions when cobalt is supported on alumina. Although it was mentioned that cobalt carbide formation is strongly kinetically inhibited, it was noted that higher partial pressures of steam enhance carbidization in keeping with the findings in the present work.

Following the removal of the carbide phase with hydrogen at 350 °C, the Co(4)Mn/CNF catalyst was exposed to FTS conditions without co-feeding of steam. Different from the freshly reduced sample where exposure to a FTS feed mixture did not lead to structural changes, such exposure of the re-reduced catalyst initially treated under humid FTS conditions led to the formation of cobalt carbide. Fig. 8 shows that a cobalt carbide doublet already appears after 6 h on stream under these mild conditions. Following 48 h under FTS conditions, the spectral contribution of the carbide doublet increased to 25%, which is even higher than it was before re-reduction. Comparing the contributions of the two metallic cobalt phases, the formation of cobalt carbide mainly led to a decrease in the bulk metallic phase. The spectral contribution of this sextuplet dropped from 40% to 22% under FTS conditions, whereas the SPM contribution only decreased by 6%.

3.2.1. Understanding carbidization under FTS conditions

The above findings indicate that the steam treatment and re-reduction resulted in a larger propensity to carbidization of cobalt in the presence of manganese. Additional experiments to gain further insight into this aspect involved the exposure of a freshly reduced Co(4)Mn/CNF catalyst to a mixture of H_2O/H_2 without CO, followed by replacing the feed by a CO/H_2 mixture. This led to the formation of cobalt carbide as shown in Fig. S5. From this, we infer that the observed more pronounced carbidization is caused by the high steam partial pressure under reducing conditions. From the finding that a catalyst, partially carbidized under

Table 1
Fit parameters of Mössbauer spectra of the Co(4)Mn/CNF catalyst after different treatments.

Treatment	Temperature (°C)	Cobalt phase	Isomer Shift (mm s^{-1})	Hyperfine Field (kOe)	Quadrupole Splitting (mm s^{-1})	Spectral Contribution (%)
After reduction	20	Co(0) SPM	0.2	–	–	76
		Co(0) bulk	−0.1	292	–	17
		Co^{2+}	1.0	–	2.0	7
During FT reaction	200	Co(0) SPM	0.0	–	–	100
RH = 7.5%	200	Co(0) SPM	−0.1	–	–	100
RH = 14%	200	Co(0) SPM	−0.1	–	–	88
		Co_2C	0.0	–	0.8	12
RH = 20%	200	Co(0) SPM	−0.1	–	–	88
		Co_2C	0.0	–	0.8	12
RH = 25%	200	Co(0) SPM	−0.1	–	–	82
		Co_2C	0.0	–	0.8	18
RH = 57%	200	Co(0) SPM	−0.1	–	–	66
		Co(0) bulk	−0.2	281	–	15
		Co_2C	0.0	–	0.9	19
After reaction	20	Co(0) SPM	0.0	–	–	63
		Co(0) bulk	−0.1	298	–	17
		Co_2C	0.1	–	0.8	20
Reduced	20	Co(0) SPM	0.0	–	–	60
		Co(0) bulk	−0.1	314	–	40

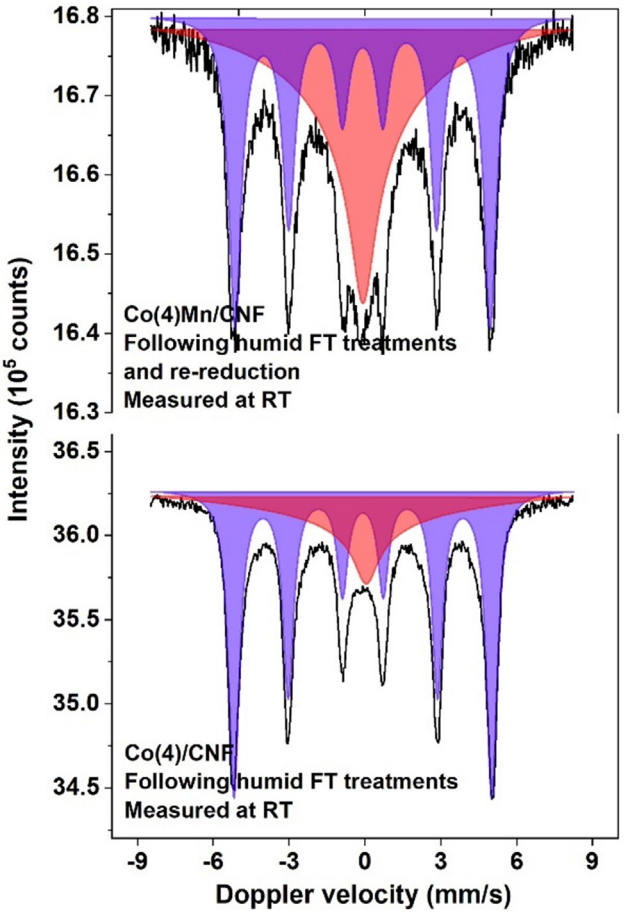

Fig. 7. Mössbauer spectra measured on Co(4)Mn/CNF and Co(4)/CNF following the humid FTS treatments: black lines represent the experimental spectra, red the fitted metallic cobalt SPM singlet, and blue the fitted bulk metallic cobalt sextuplet. (For interpretation of the references to colour in this figure legend, the reader is referred to the web version of this article.)

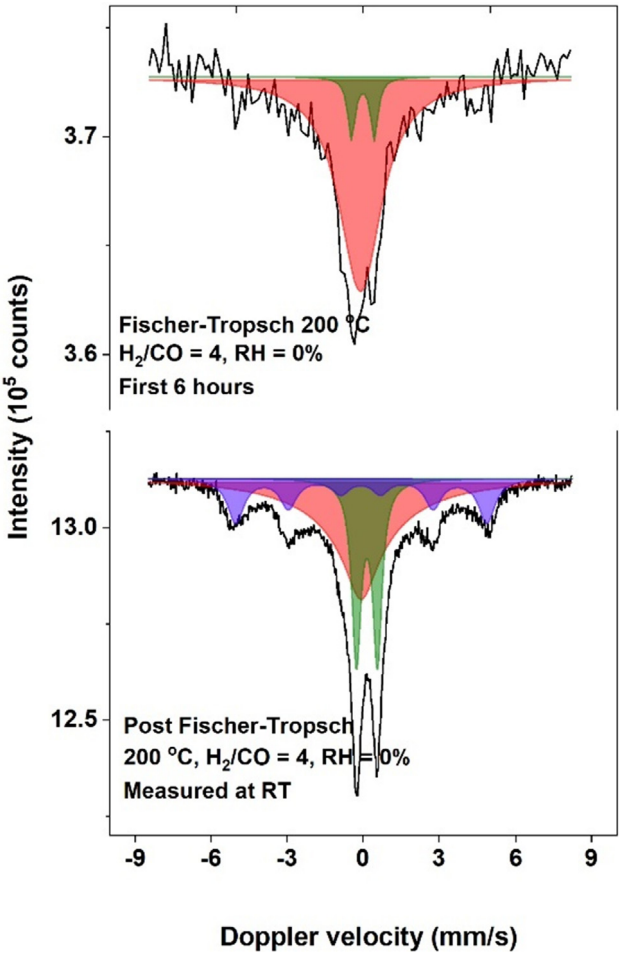

Fig. 8. *In situ* Mössbauer spectra measured on the Co(4)Mn/CNF catalyst during dry Fischer-Tropsch conditions: black lines represent the experimental spectra, red the fitted metallic cobalt SPM singlet, blue the fitted bulk metallic cobalt sextuplet, and green the fitted cobalt carbide doublet. (For interpretation of the references to colour in this figure legend, the reader is referred to the web version of this article.)

humid FTS conditions and subsequently re-reduced, formed the same carbide phase under FTS conditions without steam co-feeding (Fig. 8), we can infer that the change that induces carbidization cannot be reversed by a reduction step. Following a recent report that reduction–oxidation-reduction (ROR) treatment can lead to the redispersion of the metallic cobalt particles [4,7,12], a freshly reduced Co(4)Mn/CNF catalyst was exposed to a mixture of H_2O/H_2 in inert. Subsequently, the catalyst was exposed to a high partial pressure of steam in inert. In this oxidizing environment, the metallic cobalt particles were fully oxidized as can be appreciated from Fig. S6. Following this oxidation step, the catalyst was re-reduced in pure hydrogen and subsequently exposed to FTS conditions without steam co-feeding. The resulting spectra also given in Fig. S6 show that no carbide was formed under these conditions. This indicates that the changes in the structure caused by the high partial pressures of steam are reversible by a ROR treatment, potentially through the redispersion of the cobalt particles on the support or a reduced manganese-cobalt interaction.

We also investigated the tendency of carbidization for the Co(10)Mn/CNF catalyst. The Mössbauer spectrum of the reduced catalyst contains two contributions of metallic cobalt in the form of small and large particles (Fig. 2). Compared to Co(4)Mn/CNF, this sample contains a contribution of larger metallic cobalt particles, in line with the larger particle size determined by TEM. The *in situ* spectra measured during the various humidity treatments are given in Fig. 9, while the Mössbauer fit parameters are listed in Table S7. Different from Co(4)Mn/CNF, the cobalt carbide doublet for this sample was already observed at the lowest relative humidity of 7.5%. While the spectral parameters of this cobalt carbide doublet (IS = 0.0 mm s^{-1}, QS = 0.8 mm s^{-1}) are the same as those observed for the partially carbidized Co(4)Mn/CNF sample, the relative fraction of this cobalt carbide phase is larger for the Co(10)Mn/CNF sample (Fig. 10). As before, it is observed that the degree of carbidization increases with relative humidity, further underpinning the role of steam in carbidization. Table S7 also shows that the HF of the sextuplet contribution representing larger metallic Co particles decreases during these humidity treatments. This agrees with the earlier conclusion that especially relatively large metallic cobalt particles within the fraction of magnetically ordered cobalt particles are prone to carbidisation.

3.3. Characterization of used catalysts

The catalysts were also characterized after the *in situ* Mössbauer spectroscopy measurements. For this, nonradioactive samples exposed to the same conditions as the radioactive samples were used placed in the same cell. Representative TEM images of the used catalysts are given in Fig. 11. While small cobalt nanoparticles are observed for all catalysts, the manganese-promoted samples also contain larger agglomerates of particles, some of which are well above 50 nm in size. When determining the average particle size, the individual particles that make up these agglomerates were

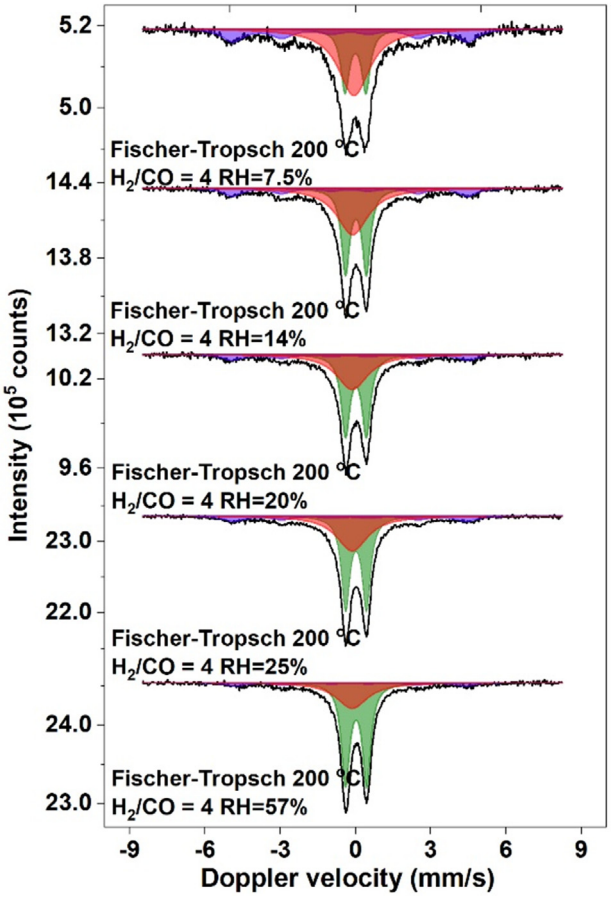

Fig. 9. *In situ* Mössbauer spectra measured of the Co(10)Mn/CNF catalyst during Fischer-Tropsch conditions under increasing humidity: black lines represent the experimental spectra, red the fitted metallic cobalt SPM singlet, blue the fitted bulk metallic cobalt sextuplet, and green the fitted cobalt carbide doublet. (For interpretation of the references to colour in this figure legend, the reader is referred to the web version of this article.)

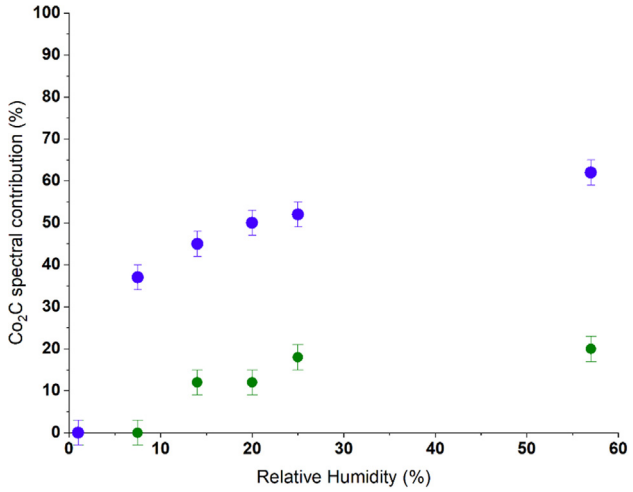

Fig. 10. Spectral contribution of cobalt carbide during increasingly humid Fischer-Tropsch conditions: the green circles show the spectral contribution measured for the Co(4)Mn/CNF catalyst, and the blue circles show the spectral contribution for the Co(10)Mn/CNF catalyst. Error bars show the experimental uncertainty of the calculated spectral contribution. (For interpretation of the references to colour in this figure legend, the reader is referred to the web version of this article.)

measured. Additionally, care was taken to distinguish between manganese oxide and cobalt particles by looking at the shape and contrast, as well as using EDX information. The average particle size for the used Co(4)/CNF and Co(4)Mn/CNF catalysts were 10.7 ± 6.6 nm and 11.6 ± 6.8 nm, respectively. This evidences that the cobalt phase has sintered in both catalysts. For the Co(10)Mn/CNF catalyst, the average particle size was 13.7 ± 7.7 nm, implying relatively speaking a smaller impact of the treatment on the initially larger particles.

To better understand cobalt carbidization, EDX measurements were performed on fresh and used Co(4)Mn/CNF and Co(10)Mn/CNF catalysts. For each of these four samples, approximately 10 different EDX maps were measured on various spots of the sample to ensure the measurements were representative for their respective catalyst. EDX maps obtained on the freshly reduced and passivated Co(10)Mn/CNF catalysts are given in Fig. 12. These maps show the proximity between cobalt and manganese with manganese being homogeneously dispersed on the support surface. Cobalt is present as nanoparticles with a size of about 10 nm with strong interactions with the manganese oxide promotor. The EDX maps in Fig. 13 for the used Co(10)Mn/CNF are very different. This catalyst contains manganese oxide particles with sizes larger than 100 nm. Three of such large manganese oxide particles were observed in the 10 EDX maps obtained for this catalyst. These large particles interact with few cobalt particles. Consequently, large parts of the carbon support surface have become relatively poor in manganese oxide. Similar findings were observed for the used Co(4)Mn/CNF catalyst, which showed two very large manganese oxide particles on the 10 measured EDX maps. Their size was smaller than in the Co(10)Mn/CNF catalyst, which can be explained by the lower manganese content of the former. These maps provide a clearer understanding of the effects that humid FTS conditions have on the catalyst morphology. Not only cobalt but also manganese oxide appears to be mobile under humid FTS conditions. The high mobility of manganese oxide results in significant sintering into large particles, which exhibit a strong interaction with part of the metallic cobalt particles. It has been shown that the proximity of Co and Mn in the precursor facilitates the formation of cobalt carbide under FTS conditions [53]. Thus, we speculate that the larger cobalt particles that strongly interact with manganese oxide are carbidized under humid FTS conditions. Furthermore, these images as well as the TEM analysis suggest that promotion with manganese oxide does not limit cobalt mobility to a significant extent on the carbon support. Whilst the presence of manganese oxide allows more of the cobalt to remain small as supported by the Mössbauer findings, the bulk particles sinter to a similar extent and are subsequently carbidized under reactive conditions.

Quasi in situ XPS was used to further investigate the apparent sintering of the used catalysts. These results, given in Fig. S8 and Table S9, show the decrease in Co/C peak ratio for every used catalyst compared to their respective fresh counterpart. Additionally, for every catalyst a higher DOR after use was observed. These two findings indicate that indeed, all catalysts experienced sintering during the humid Mössbauer treatments.

3.4. Catalytic activity measurements

Besides catalytic activity measurements in the *in situ* MES cell, the performance of the cobalt catalysts was measured in a high-pressure plug-flow reactor at 220 °C, 20 bar, a H_2/CO ratio of 4, and a gas hourly space velocity of 6500 h^{-1}. The results for the fresh and used catalysts are collected in Table 2. Fig. 14 plots the measured CTY values for the freshly reduced and used catalysts, alongside previously obtained values from literature [18] on similar carbon nanofiber supported cobalt catalysts measured at 220 °C, 1 bar and a H_2/CO ratio of 2. Turnover frequencies (TOFs)

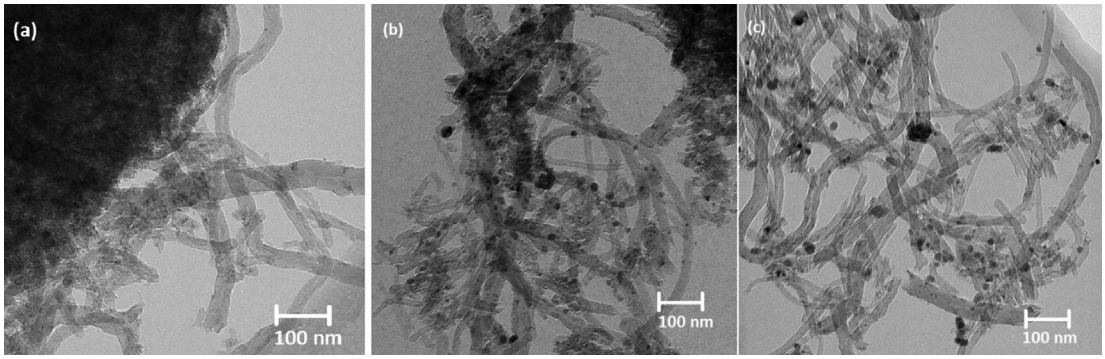

Fig. 11. Representative TEM images of used (a) Co(4)/CNF, (b) Co(4)Mn/CNF, and (c) Co(10)Mn/CNF.

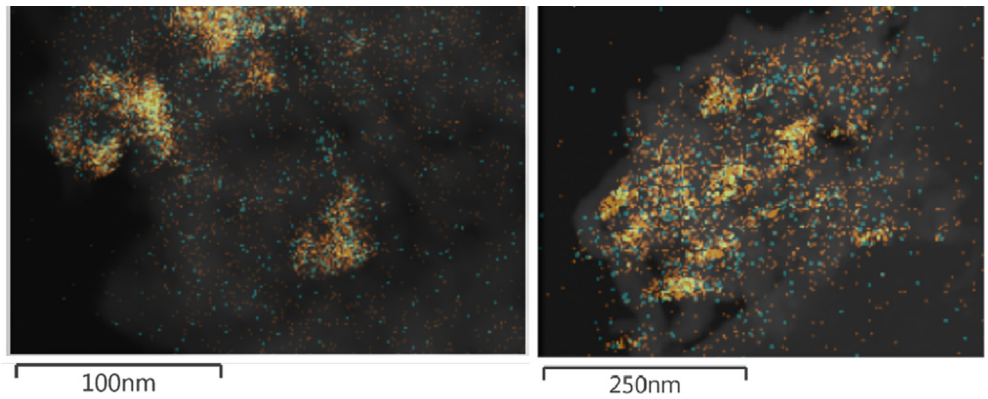

Fig. 12. EDX mappings of a reduced and passivated Co(10)Mn/CNF catalyst: the manganese mapping is shown in teal and the cobalt mapping in orange. (For interpretation of the references to colour in this figure legend, the reader is referred to the web version of this article.)

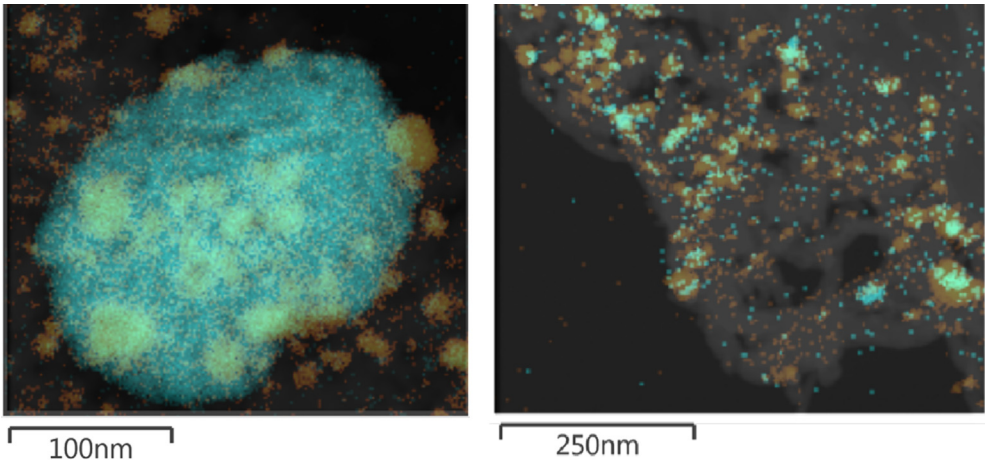

Fig. 13. EDX mappings of a used Co(10)Mn/CNF catalyst: the manganese mapping is shown in teal and the cobalt mapping in orange. (For interpretation of the references to colour in this figure legend, the reader is referred to the web version of this article.)

Table 2
Catalytic performance data for the cobalt catalysts (plug-flow reactor operated at 220 °C, 20 bar and H_2/CO = 4, GHSV = 6500 h^{-1}).

Catalyst	Conversion (%)	C_1 selectivity (%)	C_2-C_4 selectivity (%)	C_{5+} selectivity (%)	CTY (10^{-5} mol_{CO} g_{Co}^{-1} s^{-1})	TOF[a] (10^{-3} s^{-1})
Co(4)/CNF	2	27	9	64	2.2	4.7
Co(4)/CNF used	3	16	8	76	1.8	10.3
Co(4)Mn/CNF	7	21	8	71	1.0	3.0
Co(4)Mn/CNF used	3	10	8	82	2.1	–
Co(10)Mn/CNF	4	19	14	67	0.93	5.9
Co(10)Mn/CNF used	8	8	15	77	1.9	–

[a] TOF was based on the dispersion found by TEM, assuming spherical particles.

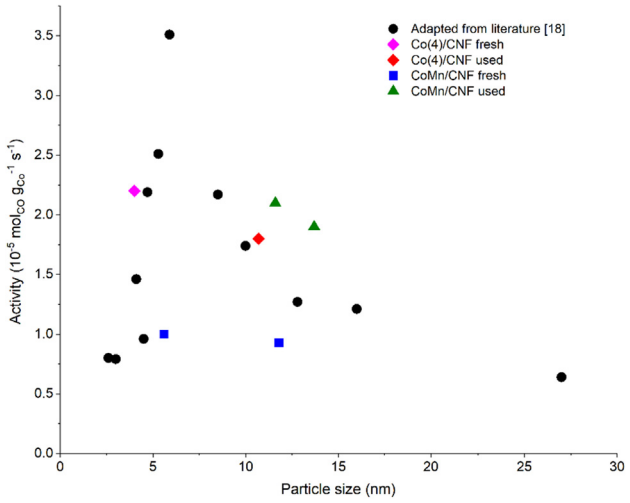

Fig. 14. Correlation between the activity of carbon-supported cobalt catalysts and their particle size. In black previously reported activities adapted from literature [18], in magenta Co(4)/CNF fresh, in red Co(4)/CNF used, in blue Co(4)Mn/CNF and Co(10)Mn/CNF fresh, and in olive Co(4)Mn/CNF and Co(10)Mn/CNF used. (For interpretation of the references to colour in this figure legend, the reader is referred to the web version of this article.)

were determined for all freshly reduced catalysts as well as the non-promoted Co(4)/CNF catalyst based on the average particle size determined by TEM assuming spherical particle shape. We do not report TOFs for the used Co(4)Mn/CNF and Co(10)Mn/CNF catalysts, because these samples contain an appreciable amount of cobalt carbide.

The Co(4)/CNF catalysts shows the expected loss in CTY activity after being exposed to humid FTS conditions, which can be explained by sintering of the metallic cobalt under humid FTS conditions. The activity only decreasing 20% versus an increase of the average cobalt particle size from 4.0 to 10.7 nm can be rationalized by the cobalt particle size effect. Upon sintering of cobalt particles smaller than 6–8 nm, the TOF of the surface atoms increases in accordance to the relation between catalytic activity and cobalt particle size [18]. The manganese-promoted catalysts show a significantly lower activity than the unpromoted catalyst after reduction. However, one would expect a higher activity given the presence of larger particles in Co(4)Mn/CNF in comparison to Co(4)/CNF. Nevertheless, it has been established before that manganese can be present on the cobalt surface lowering the FT activity through overpromotion. For instance, manganese promotion of Co/CNF (cobalt-to-manganese ratio of 10) led to a decrease of the activity by 35% [32]. The cobalt-to-manganese ratio in the present study is higher, providing a possible explanation for the significant activity decrease of the freshly reduced catalyst as well as a lower TOF despite a more optimal cobalt particle size. After use under humid FTS conditions and despite an increase of the cobalt particle size, the catalytic activity of the Co(4)Mn/CNF sample was twice that of the freshly reduced catalyst. Two explanations can be put forward. First, the increase in the cobalt particle size will increase the intrinsic activity through the particle size effect. Second, manganese migration as evidenced from TEM analysis can explain this difference. As manganese agglomerated into large clusters, the residual catalyst surface would come much closer to the optimum cobalt-to-manganese ratio for activity, which was found to be around 100 [32]. An indication that cobalt and manganese are still associated in the used catalyst follows from the lower methane selectivity compared to the non-promoted catalyst. These findings are in keeping with the notion that manganese is a promoter for the activity of cobalt FTS catalysts at low surface concentrations [32,51,54].

The Co(10)Mn/CNF catalyst showed a similar activity increase upon use as the Co(4)Mn/CNF catalyst. A closer look reveals an interesting trend in the selectivity data. In the series tested, both Co(10)Mn/CNF samples had significantly increased C_2-C_4 selectivity compared to the other ones. Such a difference has been earlier reported under 20 bar FTS conditions for overpromoted catalysts but was accompanied with a higher methane selectivity. In this series, the methane selectivity was lowest for the sample with highest manganese content. Moreover, the increased C_2-C_4 selectivity was at expense of the C_{5+} selectivity, which can be beneficial for obtaining of light olefins.

Comparing the selectivity data in Table 2, all used catalysts show an increase in C_{5+} selectivity compared to their fresh counterparts, which goes together with a decrease in the methane selectivity. It is well known that larger cobalt particles are more selective to longer hydrocarbons, while small cobalt nanoparticles are more selective to methane ([18]). The differences noted between our catalysts can be explained by the sintering under FTS conditions. Specifically for the manganese-promoted catalysts, the decrease of the negative effects of manganese overpromotion will also contribute to the improved C_{5+} selectivity.

4. Conclusions

The use of *in situ* Mössbauer spectroscopy showed a synergy between carbon monoxide and steam on the sintering of manganese-free metallic cobalt particles during FTS. Sintering in the absence of either carbon monoxide or steam was much less severe compared to the case where both gases were present. This suggests enhanced mobility of cobalt in the presence of carbon monoxide and steam. No oxidation of cobalt was observed, even at the highest steam partial pressures. Mössbauer spectroscopy shows that a substantial part of the cobalt nanoparticles remains small (in the SPM phase) in the presence of the manganese promoter. While sintering was nearly absent without steam and cobalt remained completely in the metallic form, increasing steam partial pressure led to the transformation of part of the metallic cobalt phase to cobalt carbide. EDX mapping shows that these cobalt carbide particles are likely formed due to their strong interaction with manganese oxide. Such measurements also indicate the sintering of manganese oxide under humid conditions, with particles up to 100 nm being observed on the carbon nanofiber support. The cobalt carbide phase could be fully reduced into relatively large cobalt particles. The latter result confirms the suggestion from EDX that the cobalt carbide particles were already sintered compared to the cobalt precursor. Carbidization was observed to be more severe at higher cobalt and manganese loadings. Overall, carbidization presented an alternative deactivation mechanism for the manganese-promoted cobalt nanoparticle catalyst.

Declaration of Competing Interest

The authors declare that they have no known competing financial interests or personal relationships that could have appeared to influence the work reported in this paper.

Acknowledgements

The authors gratefully acknowledge financial support from Shell Global Solutions International B.V. The authors thank Dr. Mengyue Wu from the Kavli Institute at TU Delft for assistance with STEM-EDX experiments.

Appendix A. Supplementary material

Supplementary data to this article can be found online at https://doi.org/10.1016/j.jcat.2022.06.020.

References

[1] E. Iglesia, Design, synthesis, and use of cobalt-based Fischer-Tropsch synthesis catalysts, Appl. Catal. A Gen. 161 (1–2) (1997) 59–78, https://doi.org/10.1016/S0926-860X(97)00186-5.

[2] E. Rytter, N.E. Tsakoumis, A. Holmen, On the selectivity to higher hydrocarbons in Co-based Fischer-Tropsch synthesis, Catal. Today 261 (2016) 3–16, https://doi.org/10.1016/j.cattod.2015.09.020.

[3] J.P. den Breejen, P.B. Radstake, G.L. Bezemer, J.H. Bitter, V. Frøseth, A. Holmen, K.P. de Jong, On the origin of the cobalt particle size effects in Fischer–Tropsch catalysis, J. Am. Chem. Soc. 131 (20) (2009) 7197–7203, https://doi.org/10.1021/ja901006x.

[4] N.E. Tsakoumis, M. Rønning, Ø. Borg, E. Rytter, A. Holmen, Deactivation of cobalt based Fischer-Tropsch catalysts: A review, Catal. Today 154 (3–4) (2010) 162–182, https://doi.org/10.1016/j.cattod.2010.02.077.

[5] P.J. van Berge, R.C. Everson, Cobalt as an alternative Fischer-Tropsch catalyst to iron for the production of middle distillates, Stud. Surf. Sci. Catal. 107 (15) (1997) 207–212, https://doi.org/10.1016/S0167-2991(97)80336-9.

[6] D. Moodley, M. Claeys, E. van Steen, P. van Helden, D. Kistamurthy, K.-J. Weststrate, H. Niemantsverdriet, A. Saib, W. Erasmus, J. van de Loosdrecht, Sintering of cobalt during FTS: Insights from industrial and model systems, Catal. Today 342 (2020) 59–70, https://doi.org/10.1016/j.cattod.2019.03.059.

[7] E. Rytter, A. Holmen, Deactivation and regeneration of commercial type Fischer-Tropsch co-catalysts—A mini-review, Catalysts 5 (2) (2015) 478–499, https://doi.org/10.3390/catal5020478.

[8] Z. Yu, Ø. Borg, D. Chen, E. Rytter, A. Holmen, Role of surface oxygen in the preparation and deactivation of carbon nanofiber supported cobalt Fischer-Tropsch catalysts, Top. Catal. 45 (1–4) (Aug. 2007) 69–74, https://doi.org/10.1007/s11244-007-0242-7.

[9] M. Claeys, M.E. Dry, E. van Steen, P.J. van Berge, S. Booyens, R. Crous, P. van Helden, J. Labuschagne, D.J. Moodley, A.M. Saib, Impact of Process Conditions on the Sintering Behavior of an Alumina-Supported Cobalt Fischer-Tropsch Catalyst Studied with an in Situ Magnetometer, ACS Catal. 5 (2) (2015) 841–852, https://doi.org/10.1021/cs501810y.

[10] M.D. Argyle, T.S. Frost, C.H. Bartholomew, Cobalt Fischer-Tropsch catalyst deactivation modeled using generalized power law expressions, Top. Catal. 57 (6–9) (2014) 415–429, https://doi.org/10.1007/s11244-013-0197-9.

[11] M. Rahmati, M.-S. Safdari, T.H. Fletcher, M.D. Argyle, C.H. Bartholomew, Chemical and thermal sintering of supported metals with emphasis on cobalt catalysts during Fischer-Tropsch synthesis, Chem. Rev. 120 (10) (2020) 4455–4533, https://doi.org/10.1021/acs.chemrev.9b00417.

[12] C.E. Kliewer, S.L. Soled, G. Kiss, Morphological transformations during Fischer-Tropsch synthesis on a titania-supported cobalt catalyst, Catal. Today 323 (Feb. 2019) 233–256, https://doi.org/10.1016/j.cattod.2018.05.021.

[13] T.O. Eschemann, K.P. de Jong, Deactivation Behavior of Co/TiO_2 Catalysts during Fischer-Tropsch Synthesis, ACS Catal. 5 (6) (Jun. 2015) 3181–3188, https://doi.org/10.1021/acscatal.5b00268.

[14] M. Wolf, E.K. Gibson, E.J. Olivier, J.H. Neethling, C.R.A. Catlow, N. Fischer, M. Claeys, In-depth characterisation of metal-support compounds in spent Co/SiO_2 Fischer-Tropsch model catalysts, Catal. Today 342 (2020) 71–78, https://doi.org/10.1016/j.cattod.2019.01.065.

[15] W. Zhou, J.-G. Chen, K.-G. Fang, Y.-H. Sun, The deactivation of Co/SiO_2 catalyst for Fischer-Tropsch synthesis at different ratios of H_2 to CO, Fuel Process. Technol. 87 (7) (Jul. 2006) 609–616, https://doi.org/10.1016/j.fuproc.2006.01.008.

[16] G.L. Bezemer, T.J. Remans, A.P. van Bavel, A.I. Dugulan, Direct evidence of water-assisted sintering of cobalt on carbon nanofiber catalysts during simulated Fischer–Tropsch conditions revealed with in situ mössbauer spectroscopy, J. Am. Chem. Soc. 132 (25) (Jun. 2010) 8540–8541, https://doi.org/10.1021/ja103002k.

[17] Z. Yu, Ø. Borg, D.e. Chen, B.C. Enger, V. Frøseth, E. Rytter, H. Wigum, A. Holmen, Carbon nanofiber supported cobalt catalysts for Fischer-Tropsch synthesis with high activity and selectivity, Catal. Lett. 109 (1-2) (2006) 43–47, https://doi.org/10.1007/s10562-006-0054-6.

[18] G.L. Bezemer, J.H. Bitter, H.P.C.E. Kuipers, H. Oosterbeek, J.E. Holewijn, X. Xu, F. Kapteijn, A.J. van Dillen, K.P. de Jong, Cobalt particle size effects in the Fischer-Tropsch reaction studied with carbon nanofiber supported catalysts, J. Am. Chem. Soc. 128 (12) (2006) 3956–3964, https://doi.org/10.1021/ja058282w.

[19] E. Van Steen, M. Claeys, M.E. Dry, J. Van De Loosdrecht, E.L. Viljoen, J.L. Visagie, Stability of nanocrystals: Thermodynamic analysis of oxidation and re-reduction of cobalt in water/hydrogen mixtures, J. Phys. Chem. B 109 (8) (2005) 3575–3577, https://doi.org/10.1021/jp045136o.

[20] J. van de Loosdrecht, B. Balzhinimaev, J.-A. Dalmon, J.W. Niemantsverdriet, S.V. Tsybulya, A.M. Saib, P.J. van Berge, J.L. Visagie, Cobalt Fischer-Tropsch synthesis: Deactivation by oxidation?, Catal Today 123 (1-4) (2007) 293–302, https://doi.org/10.1016/j.cattod.2007.02.032.

[21] H. Karaca, O.V. Safonova, S. Chambrey, P. Fongarland, P. Roussel, A. Griboval-Constant, M. Lacroix, A.Y. Khodakov, Structure and catalytic performance of Pt-promoted alumina-supported cobalt catalysts under realistic conditions of Fischer-Tropsch synthesis, J. Catal. 277 (1) (2011) 14–26, https://doi.org/10.1016/j.jcat.2010.10.007.

[22] M. Wolf, B.K. Mutuma, N.J. Coville, N. Fischer, M. Claeys, Role of CO in the water-induced formation of cobalt oxide in a high conversion Fischer-Tropsch environment, ACS Catal. 8 (5) (2018) 3985–3989, https://doi.org/10.1021/acscatal.7b0417710.1021/acscatal.7b04177.s001.

[23] M. Sadeqzadeh, J. Hong, P. Fongarland, D. Curulla-Ferré, F. Luck, J. Bousquet, D. Schweich, A.Y. Khodakov, Mechanistic modeling of cobalt based catalyst sintering in a fixed bed reactor under different conditions of Fischer-Tropsch synthesis, Ind. Eng. Chem. Res. 51 (37) (2012) 11955–11964, https://doi.org/10.1021/ie3006929.

[24] M. Claeys, M.E. Dry, E. van Steen, E. du Plessis, P.J. van Berge, A.M. Saib, D.J. Moodley, In situ magnetometer study on the formation and stability of cobalt carbide in Fischer-Tropsch synthesis, J. Catal. 318 (2014) 193–202, https://doi.org/10.1016/j.jcat.2014.08.002.

[25] G. Jacobs, P.M. Patterson, Y. Zhang, T. Das, J. Li, B.H. Davis, Fischer–Tropsch synthesis: deactivation of noble metal-promoted Co/Al_2O_3 catalysts, Appl. Catal. A Gen. 233 (1–2) (Jul. 2002) 215–226, https://doi.org/10.1016/S0926-860X(02)00147-3.

[26] H. Karaca, J. Hong, P. Fongarland, P. Roussel, A. Griboval-Constant, M. Lacroix, K. Hortmann, O.V. Safonova, A.Y. Khodakov, In situ XRD investigation of the evolution of alumina-supported cobalt catalysts under realistic conditions of Fischer-Tropsch synthesis, Chem. Commun. 46 (5) (2010) 788–790, https://doi.org/10.1039/B920110F.

[27] H.H. Storch, N. Golumbic, R.B. Anderson, The Fischer-Tropsch and Related Syntheses, Wiley, New York, 1951.

[28] M. van der Riet, G.J. Hutchings, R.G. Copperthwaite, Selective formation of C_3 hydrocarbons from CO + H_2 using cobalt–manganese oxide catalysts, J. Chem. Soc., Chem. Commun. 10 (1986) 798–799, https://doi.org/10.1039/C39860000798.

[29] S. Colley, R.G. Copperthwaite, G.J. Hutchings, M. Van der Riet, Carbon monoxide hydrogenation using cobalt manganese oxide catalysts: initial catalyst optimization studies, Ind. Eng. Chem. Res. 27 (8) (Aug. 1988) 1339–1344, https://doi.org/10.1021/ie00080a001.

[30] G.J. Hutchings, M. van der Riet, R. Hunter, CO hydrogenation using cobalt/manganese oxide catalysts. Comments on the mechanism of carbon–carbon bond formation, J. Chem. Soc., Faraday Trans. 1 85 (9) (1989) 2875, https://doi.org/10.1039/f19898502875.

[31] S.E. Colley, R.G. Copperthwaite, G.J. Hutchings, S.P. Terblanche, M.M. Thackeray, Identification of body-centred cubic cobalt and its importance in CO hydrogenation, Nature 339 (6220) (May 1989) 129–130, https://doi.org/10.1038/339129a0.

[32] G. Bezemer, P. Radstake, U. Falke, H. Oosterbeek, H. Kuipers, A. Vandillen, K. Dejong, Investigation of promoter effects of manganese oxide on carbon nanofiber-supported cobalt catalysts for Fischer-Tropsch synthesis, J. Catal. 237 (1) (2006) 152–161, https://doi.org/10.1016/j.jcat.2005.10.031.

[33] F. Morales, F.M.F. de Groot, P. Glatzel, E. Kleimenov, H. Bluhm, M. Hävecker, A. Knop-Gericke, B.M. Weckhuysen, In situ X-ray absorption of Co/Mn/TiO_2 catalysts for fischer-tropsch synthesis, J. Phys. Chem. B 108 (41) (2004) 16201–16207, https://doi.org/10.1021/jp0403846.

[34] F. Morales, F. De Groot, O. Gijzeman, A. Mens, O. Stephan, B. Weckhuysen, Mn promotion effects in Co/TiO_2 Fischer-Tropsch catalysts as investigated by XPS and STEM-EELS, J. Catal. 230 (2) (Mar. 2005) 301–308, https://doi.org/10.1016/j.jcat.2004.11.047.

[35] A.Y. Khodakov, W. Chu, P. Fongarland, Advances in the development of novel cobalt Fischer-Tropsch catalysts for synthesis of long-chain hydrocarbons and clean fuels, Chem. Rev. 107 (5) (2007) 1692–1744, https://doi.org/10.1021/cr050972v.

[36] M.W.J. Crajé, A.M. Van der Kraan, J. Van de Loosdrecht, P.J. Van Berge, The application of Mössbauer emission spectroscopy to industrial cobalt based Fischer-Tropsch catalysts, Catal. Today 71 (3–4) (2002) 369–379, https://doi.org/10.1016/S0920-5861(01)00464-3.

[37] M.K. Van Der Lee, A. Van Jos Dillen, J.H. Bitter, K.P. De Jong, Deposition precipitation for the preparation of carbon nanofiber supported nickel catalysts, J. Am. Chem. Soc. 127 (39) (2005) 13573–13582, https://doi.org/10.1021/ja053038q.

[38] Z. Klencsár, MossWinn—methodological advances in the field of Mössbauer data analysis, Hyperfine Interact. 217 (1–3) (Apr. 2013) 117–126, https://doi.org/10.1007/s10751-012-0732-2.

[39] M. Blume, J.A. Tjon, Mössbauer Spectra in a Fluctuating Environment, Phys. Rev. 165 (2) (1968) 446–456, https://doi.org/10.1103/PhysRev.165.456.

[40] G.K. Wertheim, Hyperfine Structure of Divalent and Trivalent Fe^{57} in Cobalt Oxide, Phys. Rev. 124 (3) (1961) 764–767, https://doi.org/10.1103/PhysRev.124.764.

[41] G.K. Wertheim, Chemical Effects of Nuclear Transformations in Mössbauer Spectroscopy, Acc. Chem. Res. 4 (11) (1971) 373–379, https://doi.org/10.1021/ar50047a003.

[42] H. Pollak, Fe^{3+} Ion Lifetime in CoO Deduced from the Auger and Mössbauer Effects, Phys. State. Sol. 2 (6) (1962) 720–724, https://doi.org/10.1002/pssb.19620020609.

[43] A. Cruset, J.M. Friedt, Mossbauer Study of the Valence State of ^{57}Fe after ^{57}Co Decay in $CoFe_2O_4$, Phys. State. Sol. 45 (1971) 189, https://doi.org/10.1002/pssb.2220450120.

[44] C. Wivel, B.S. Clausen, R. Candia, S. Mørup, H. Topsøe, Mössbauer Emission Studies of Calcined Co-Mo/Al_2O_3 Catalysts: Catalytic Signifcance of the Co Precursors, J. Catal. 87 (1984) 497–513, https://doi.org/10.1016/0021-9517(84)90210-0.

[45] H. Topsoe, B.S. Clausen, R. Candia, C. Wivel, S. Mørup, In situ Mössbauer emission spectroscopy studies of unsupported and supported sulfided Co-Mo hydrodesulfurization catalysts: Evidence for and nature of a Co-Mo-S phase, J. Catal. 68 (2) (1981) 433–452, https://doi.org/10.1016/0021-9517(81)90114-7.

[46] J.A.R. Van Veen, E. Gerkema, A.M. Van Der Kraan, P.A.J.M. Hendriks, H. Beens, A ^{57}CO Mössbauer emission spectrometric study of some supported CoMo hydrodesulfurization catalysts, J. Catal. 133 (1) (Jan. 1992) 112–123, https://doi.org/10.1016/0021-9517(92)90189-O.

[47] M.W.J. Crajé, V.H.J. De Beer, J.A.R. Van Veen, A.M. Van Der Kraan, Sulfidation of Co/Al_2O_3 and CoMo/Al_2O_3 catalysts studied by mössbauer emission spectroscopy, J. Catal. 143 (2) (1993) 601–615, https://doi.org/10.1006/jcat.1993.1303.

[48] F. Morales, D. Grandjean, A. Mens, F.M.F. de Groot, B.M. Weckhuysen, X-ray Absorption Spectroscopy of Mn/Co/TiO_2 Fischer−Tropsch Catalysts: Relationships between Preparation Method, Molecular Structure, and Catalyst Performance, J. Phys. Chem. B 110 (17) (May 2006) 8626–8639, https://doi.org/10.1021/jp0565958.

[49] M. Wolf, N. Fischer, M. Claeys, Water-induced deactivation of cobalt-based Fischer-Tropsch catalysts, Nat. Catal. 3 (12) (Dec. 2020) 962–965, https://doi.org/10.1038/s41929-020-00534-5.

[50] M. Wolf, N. Fischer, M. Claeys, Capturing the interconnectivity of water-induced oxidation and sintering of cobalt nanoparticles during the Fischer-Tropsch synthesis in situ, J. Catal. 374 (Jun. 2019) 199–207, https://doi.org/10.1016/j.jcat.2019.04.030.

[51] F. Morales, E. de Smit, F.M.F. de Groot, T. Visser, B.M. Weckhuysen, Effects of manganese oxide promoter on the CO and H_2 adsorption properties of titania-supported cobalt Fischer-Tropsch catalysts, J. Catal. 246 (1) (2007) 91–99, https://doi.org/10.1016/j.jcat.2006.11.014.

[52] F.R. Van den Berg, M.W.J. Crajé, A.M. Van der Kraan, J.W. Geus, Reduction behaviour of Fe/ZrO_2 and Fe/K/ZrO_2 Fischer-Tropsch catalysts, Appl. Catal. A Gen. 242 (2) (2003) 403–416, https://doi.org/10.1016/S0926-860X(02)00532-X.

[53] Z. Li, L. Zhong, F. Yu, Y. An, Y. Dai, Y. Yang, T. Lin, S. Li, H. Wang, P. Gao, Y. Sun, M. He, Effects of Sodium on the Catalytic Performance of CoMn Catalysts for Fischer-Tropsch to Olefin Reactions, ACS Catal. 7 (5) (2017) 3622–3631, https://doi.org/10.1021/acscatal.6b0347810.1021/acscatal.6b03478.s001.

[54] J.P. den Breejen, A.M. Frey, J. Yang, A. Holmen, M.M. van Schooneveld, F.M.F. de Groot, O. Stephan, J.H. Bitter, K.P. de Jong, A highly active and selective manganese oxide promoted cobalt-on-silica Fischer-Tropsch catalyst, Top. Catal. 54 (13-15) (2011) 768–777, https://doi.org/10.1007/s11244-011-9703-0.